Coupled subdaily and multiweek cycles during the lava dome erupt of Soufriere Hills Volcano, Montserrat

Article

Published Version

Coupled subdaily and multiweek cycles during the lava dome eruption of Soufrière Hills Volcano, Montserrat

A. Costa,[1,2,3] G. Wadge,[1] R. Stewart,[4,5] and H. Odbert[5,6]

[1]   Observations of volcanoes extruding andesitic lava to produce lava domes often reveal cyclic behavior. At Soufrière Hills Volcano, Montserrat, cycles with subdaily and multiweek periods have been recognized on many occasions. Observations clearly show that the period of subdaily cycles is modulated by the multiweek cycle. The subdaily and multiweek cycles have been modeled separately as stick-slip magma flow at the junction between a dyke and an overlying cylindrical conduit and as the filling and discharge of magma through the elastic-walled dyke, respectively. Here, we couple these two models to describe the behavior over a period of well-observed multiweek cycles, with accompanying subdaily cycles, from 13 May to 21 September 1997. The coupled model captures well the asymmetrical first-order behavior: the first 40% of the multiweek cycle consists of high rates of lava extrusion during short period/high amplitude subdaily cycles as the dyke reservoir discharges itself. The remainder of the cycle involves increasing pressurization as more magma is stored, and extrusion rate falls, followed by a gradual increase in the period of the subdaily cycles.

1. Introduction

[2]   Cyclic behavior on timescales from a few to many hours during volcanic activity is of considerable interest because it provides repeatable "experiments" from an otherwise largely hidden system. Such behavior has been commonly recognized at numerous, well-monitored volcanoes (e.g., Mount St Helens [*Anderson et al.*, 2010]; Unzen [*Yamashina et al.*, 1999]; Semeru [*Nishi et al.*, 2007]). Of particular interest are those systems that show short-period cycles nested within longer-period cycles because, potentially, we can use the insights and constraints derived from the study of one type of cycle to better understand the other type and their combined behavior. One of the best studied systems with multiple cycles is the Soufrière Hills Volcano (SHV), Montserrat. To explain long-term cyclicity, *Costa et al.* [2007a, 2007b] considered an elastic dyke joined to a cylinder toward the surface, coupled with a magma chamber below (Figure 1). They showed that degassing-induced crystallization within the conduit coupled with the wall rock elasticity largely control the long-term cyclicity during lava dome–building eruptions. The model of *Costa et al.* [2007b] demonstrated that there is a regime where the period of pulsations is controlled by the elasticity of the dyke, having periods from weeks to months, and a regime where the period is controlled by the volume of the magma chamber with periods of the order of years. Intermediate regimes are possible.

[3]   Several models have been proposed to explain short-term cyclicity [for a review, see *Melnik et al.*, 2009]. The models of both *Denlinger and Hoblitt* [1999] and *Wylie et al.* [1999] assumed that the lower part of the SHV conduit acts like a capacitor that allows magma to be stored temporally to release it during the intense phase of the eruption. *Costa et al.* [2012] generalized the *Denlinger and Hoblitt* [1999] model by considering a compressible magma flowing through an elastic dyke that transitions to a cylindrical conduit near the surface (see Figure 1). *Lensky et al.* [2008] described short-term cyclicity at the SHV as a result of gas diffusion into growing bubbles and filtration through the bubble network in a stagnated magma column before the critical overpressure is reached followed by magma motion, depressurization, and stagnation of the plug at the top of the conduit.

[4]   Tiltmeter data recorded within a few hundred meters of the growing lava dome at SHV in 1997 [*Voight et al.*, 1998, 1999] demonstrated both a subdaily cycle (generally with periods in the range 3 to 30 h) and a multiweek cycle (periods mainly between 30 and 50 days) [*Sparks and Young*, 2002; *Odbert and Wadge*, 2009]. *Odbert et al.* [2013] recognized that these two cycles have been present, albeit intermittently, for most of the eruption of SHV

[1]Environmental Systems Science Centre, University of Reading, Reading, UK.
[2]Istituto Nazionale Geofisica Vulcanologia, Naples, Italy.
[3]Istituto Nazionale Geofisica Vulcanologia, Bologna, Italy.
[4]Seismic Research Centre, University of the West Indies, Trinidad and Tobago.
[5]Montserrat Volcano Observatory, Flemmings, Montserrat.
[6]School of Earth Sciences, University of Bristol, Bristol, UK.

Corresponding author: A. Costa, Istituto Nazionale Geofisica Vulcanologia, Bologna, Italy. (antonio.costa@bo.ingv.it)
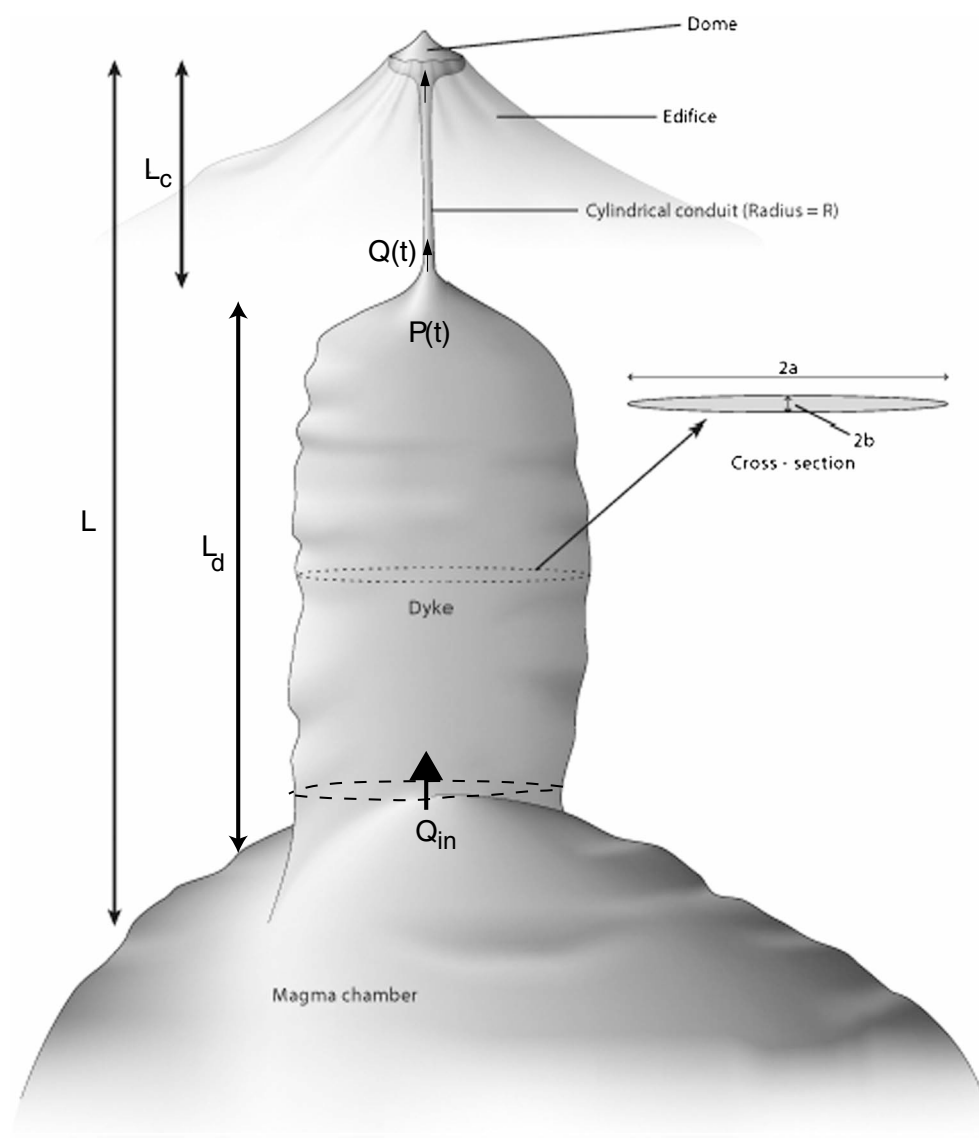
Figure 1. Simplified sketch of the investigated system [from *Costa et al.*, 2012].

between 1995 and 2010. This longevity of behavior suggests that the physical conditions that drive the cycles are quasi-permanent features of the volcano.

[5] The physical conditions during subdaily cycles are better understood than those associated with the multiweek cycles. Two main types of observation inform this. First, vulcanian explosions occurring near the peaks of the subdaily cycles, observed in August and September–October 1997, indicate pressurization beneath a plug of degassed magma within a cylindrical conduit that is then evacuated explosively [*Druitt et al.*, 2002]. Second, swarms of self-similar, hybrid (high-frequency onset with a low-frequency coda) earthquakes occurring during pressurization originate at a depth of ~1.5 km below the dome and suggest a repeating mechanism during magma flow that is confined to that depth [*Neuberg et al.*, 2006; *Green and Neuberg*, 2006]. Highly nonlinear, rheological changes within the magma in the shallower part of the conduit [*Sparks and Melnik*, 1999] coupled with a near-wall, stick-slip mechanism of flow in the deeper conduit [*Denlinger and Hoblitt*, 1999;

Lensky et al., 2008; *Costa et al.*, 2012] are thought to be responsible for these phenomena.

[6] Multiweek cycles were recognized as involving initially high extrusion rates of lava, with accompanying high rates of surface deflation, and a typical extruded volume of about $30 \times 10^6 \, \text{m}^3$ per cycle [*Sparks and Young*, 2002]. This behavior suggests a discharge-recharge process. An elastic-walled dyke (with approximate dimensions of 4 km high, 480 m wide, and ~5 m thick) joining the cylindrical conduit above and a magma reservoir below were proposed by *Costa et al.* [2007a] as the source of this process. The junction of the dyke and cylinder was invoked as the likely location of the stick-slip process postulated for the subdaily cycles and of the hybrid earthquakes [*Costa et al.*, 2012; *Thomas and Neuberg*, 2012]. The surface deformation occurring across multiweek cycles was measured both by near-field (<1 km) tiltmeters in 1997 [*Sparks and Young*, 2002] and perhaps by far-field (>2 km) cGPS receivers in 2009 [*Odbert et al.*, 2013], and this accumulated strain was not immediately recovered, as was the case for the subdaily

deformation. However, the aggregate episodes of deflation across all these multiweek cycles during lava extrusion was at least partially balanced by inflation during pauses in extrusion [e.g., *Elsworth et al.*, 2008]. Five of these multiyear cycles of extrusion and pause have occurred between 1995 and 2010, representing the third, and longest, type of cyclic behavior during the eruption at SHV [*Odbert et al.*, 2013].

[7] In this article, we argue that the sets of processes inferred for the multiweek and subdaily cycles must be coupled [*Sparks and Young*, 2002; *Odbert et al.*, 2013]. We use modified forms of the two physical models that have been used to simulate cyclic behavior at the multiweek [*Costa et al.*, 2007a] and the subdaily [*Costa et al.*, 2012] scales to represent this coupled behavior. We compare the coupled model with observations from SHV, particularly between May and September 1997.

2. Coupled Cyclic Behavior

[8] This interpretation of the two cycles requires that the varying physical conditions imposed by the discharge-recharge cycle of the dyke will modulate the conditions of the subdaily cycle, and hence the characteristics of the subdaily cycle should change systematically through the longer cycle. This, generally, is what we observe. Figure 2 shows the average period of the subdaily cycles across eight selected multiweek cycles of normalized duration (40 days).

[9] The multiweek cycles usually start abruptly. A hiatus in flow from one cycle to the next is sometimes manifested as a change in direction of the extrusion of lava on the dome and/or the generation of a spine [*Watts et al.*, 2002]. This is then followed by elevated lava extrusion rates, swarms of hybrid earthquakes, and reduced periods of the subdaily
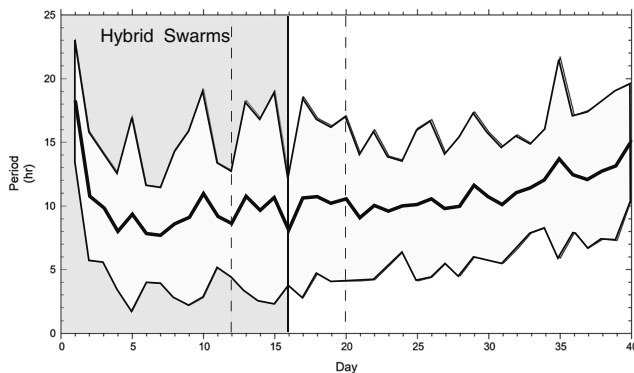

Figure 2. The variation of the period of subdaily cycles (thick black line with standard deviation envelope in pale gray) measured by seismicity averaged across eight selected multiweek cycles (28 July 1996–17 September 1996; 23 December 1996–15 February 1997; 13 May 1997–22 June 1997; 22 June 1997–31 July 1997; 31 July 1997–8 September 1997; 9 October 2009–20 November 2009; 20 November 2009–9 January 2010; and 9 January 2010–11 February 2010). The durations of the multiweek cycles are normalized to 40 days, the subdaily cycles are binned by day, and outliers are removed. The average duration and standard deviation of the initial hybrid earthquake swarms (16 ± 4 days) is shown by the darker gray panel and dashed vertical lines.

cycle. During the next 16 days or so (after approximately 40% of the period), the subdaily period reaches a minimum value, the hybrid earthquakes diminish, and after that the period rises slowly to the end of the cycle (Figure 2). The multiweek cycle is thus highly asymmetrical.

3. The Coupled Dyke-Cylinder Model

[10] In their model of the subdaily cyclicity, *Costa et al.* [2012] proposed that just above the junction between the dyke and the cylindrical conduit there is stick-slip flow of magma that behaves as a polymer in contact with the conduit wall. They devised an appropriately parameterized analytical model that yielded the observed range of subdaily cycle periods for SHV. In their analytical model, the period is proportional to a constant that depends on physical properties of the magma and geometry of the system and is inversely proportional to the combined compressibility of the magma and the rigidity of the elastic wall rocks, expressed as a compressibility-rigidity modulus, which we term here the system rigidity. Because of the short duration of the subdaily cycle, *Costa et al.* [2012] argued that this system rigidity could be treated as constant. These assumptions cannot be made for the entire duration of the longer (multiweek) period, and its temporal variation must be explicitly calculated.

[11] *Costa et al.* [2007a, 2007b] considered an elastic dyke changing to a cylinder toward the surface coupled with a shallow (~5 km deep) magma chamber. The model accounts for gas exsolution and filtration through the magma, degassing-induced crystallization kinetics, rheological stiffening of magma due to crystal growth, and latent heat release. The physical model is based on mass conservation equations for melt, microlites, phenocrysts, and dissolved and exsolved gas that are solved together with an energy equation and two momentum equations (for the mixture as a whole and the gas phase). Variations in conduit cross-sectional area due to elastic deformation of the wall rocks are also considered by assuming that the conduit has an elliptic cross section whose length is dependent on the vertical position and a transition from a thin dyke at depth to a nonelastic cylindrical conduit at shallow level. They found that different flow regimes are possible. In particular, there is a regime where the period of pulsations is controlled by the elasticity of the dyke (~weeks to months) and a regime where the period is controlled by the volume of the magma chamber (~years). Intermediate regimes are possible. The model proposed by *Costa et al.* [2007a, 2007b] is also consistent with geophysical observations [e.g., *Hautmann et al.*, 2009].

[12] We have modified the *Costa et al.* [2007a] model of multiweek flow using data from two new studies. The conduit is lengthened (from 5 to 5.5 km), following the depth to the magma reservoir estimated by *Paulatto et al.* [2012] from seismic tomography. Young's modulus (*E*), Poisson's ratio (*v*), and the shear modulus (*G*) are estimated from the one-dimensional seismic velocity profile beneath Soufriere Hills Volcano of *Paulatto et al.* [2009] (Figure 3). The shear modulus *G* is then rescaled to give an empirical relationship between the static and the dynamic values [*Wang*, 2000]. The *Costa et al.* [2007a] numerical model was then used to estimate the system rigidity and other parameters needed for the analytical estimation of the subdaily period, *T*, proposed by *Costa et al.* [2012]:

(a)

$E(x)=a \cdot \ln(b+x^c)$ ——

(b)

$v(x)=0.341+(a_1 x+a_2 x^2+a_3 x^3+a_4 x^4)\exp(-a_5 x)-0.041\exp(-a_5/x)$ ——

(c)

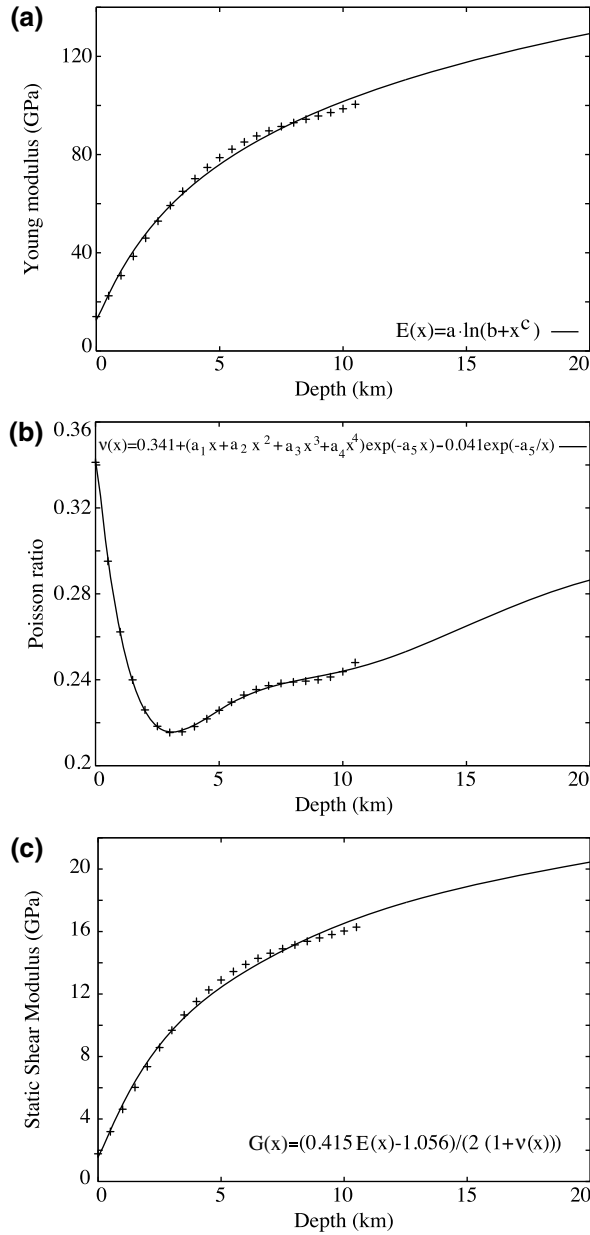
$G(x)=(0.415 E(x)-1.056)/(2 (1+v(x)))$

Figure 3. Crustal material property curves (lines) for (a) Young's modulus, (b) Poisson's ratio, and (c) static shear modulus (G), fitted to the seismic survey–derived data (crosses) of *Paulatto et al.* [2009]. The numerical values of the best fit parameters are as follows: $a = 37.01$, $b = 1.41$, $c = 1.15$; $a_1 = -0.0527$, $a_2 = -0.0344$, $a_3 = 0.00764$, $a_4 = -0.00079$, and $a_5 = 0.43$.

$$T \approx \frac{A}{\gamma} \quad (1)$$

where A is a constant that depends on physical properties of magma and geometry of the system (see Table 1), and γ is the system rigidity parameter representing an effective compressibility–rigidity modulus. Here γ is estimated using the *Costa et al.* [2007a] model and the parameters reported in Table 1 (see Appendix A), although in principle it can be expressed as a function of the magma bulk modulus, K, controlled by the presence of bubbles and pressure distribution inside the dyke,

Table 1. Parameters Used in the Models

Notation	Description	Value
c_0	Concentration of dissolved gas	5.5 wt%
C_f	Solubility coefficient	$4.1 \times 10^{-6}\,\mathrm{Pa}^{-1/2}$
C_m	Specific heat	$1.2 \times 10^3\,\mathrm{J\,kg^{-1}\,K^{-1}}$
I_0	Max nucleation rate	$3 \times 10^{10}\,\mathrm{m^{-3}\,s^{-1}}$
L_*	Latent heat of crystallization	$3.5 \times 10^5\,\mathrm{J\,kg^{-1}}$
P_{ch}	Chamber pressure	170.7 MPa
R_g	Gas constant	$460\,\mathrm{J\,kg^{-1}\,K^{-1}}$
R_{ph}	Phenocryst size	5 mm
T_{ch}	Temperature in the magma chamber	870°C
U_0	Max growth rate	$2 \times 10^{-9}\,\mathrm{m\,s^{-1}}$
β_{ch*}	Chamber crystal content	0.45
μ_g	Gas viscosity	$1.5 \times 10^{-5}\,\mathrm{Pa\,s}$
ρ_c^0	Density of crystals	$2700\,\mathrm{kg\,m^{-3}}$
ρ_m^0	Density of the melt phase	$2300\,\mathrm{kg\,m^{-3}}$
ρ_r	Density of wall rocks	$2600\,\mathrm{kg\,m^{-3}}$
L	Total conduit length	5500 m
L_c	Cylindrical conduit length	1300 m
R	Cylindrical conduit radius	15 m
A_d	Unpressurized dyke cross section	$1730\,\mathrm{m^2}$
Q_{in}	Flow rate at the dyke base	Calculated (5.5 $\mathrm{m^3\,s^{-1}}$)[a]
Q_{out}	Flow rate at the dyke base	Calculated (5.5 $\mathrm{m^3\,s^{-1}}$)[a]
V_d	Volume of the dyke region	Calculated ($7.3 \times 10^6\,\mathrm{m^3}$)[a]
ρ	Average overall magma density	Calculated (2100 $\mathrm{kg\,m^{-3}}$)[a]
μ	Viscosity in the cylinder region	Calculated ($6 \times 10^9\,\mathrm{Pa\,s}$)[a]
P_*	Average pressure drop	Calculated (10 MPa)[a]
X_*	Dimensionless fixed point	0.34 [b]
$t_* = \mu/P_*$	Characteristic timescale	612 s
$\varepsilon = \frac{\beta R P_*}{8\mu v_*} = \frac{\beta}{8}$	Dimensionless pressure parameter	0.0014
$\zeta = \frac{\gamma \pi R^3}{P_* V_d}$	Dimensionless compressibility parameter	0.023
$\alpha = a P_*^m/v_*$	Dimensionless slip parameter	10
$q_{in} = \frac{\mu Q_{in}}{\pi R^3 \rho P_*}$	Dimensionless flow rate	0.38
$A = \frac{2\mu V_d}{\alpha m R^3 X_*^{m-1}}$	Dimensional parameter	$7.47 \times 10^6\,\mathrm{Pa\,s}$

[a]Calculated from the *Costa et al.* [2007a] model. The average values are shown in parentheses.
[b]Calculated using the *Costa et al.* [2012] model.

and the rigidity modulus of rocks surrounding the dyke, G. Table 1 shows the parameters used for equation (1). Such a relationship is valid for the first-order analysis used in this article, and a more rigorous approach consisting of implementing a stick-slip mechanism directly within the *Costa et al.* [2007a] dyke model is the subject of ongoing research. The multiweek period is constrained to ~40 days for comparison with the 1997 cycles.

4. Model-Observation Comparison

[13] We now test the coupled model against seismic and tilt data and daily values of extrusion rate of lava at SHV from May to September 1997 (see Figure 4). The tiltmeter data collected from 18 May to 4 August 1997, coupled with the seismicity [*Odbert et al.*, 2013] and lava extrusion rates [*Sparks et al.*, 1998], best represent the two multiweek cycles shown by *Sparks and Young* [2002, Figure 12]. We extend that record using seismicity and extrusion rate to cover a third consecutive multiweek cycle.

4.1. 13 May–22 June 1997

[14] This cycle began with a swarm of hybrid seismicity on 13 May 1997 [*Luckett et al.*, 2008]. By 16 May, a 50 m
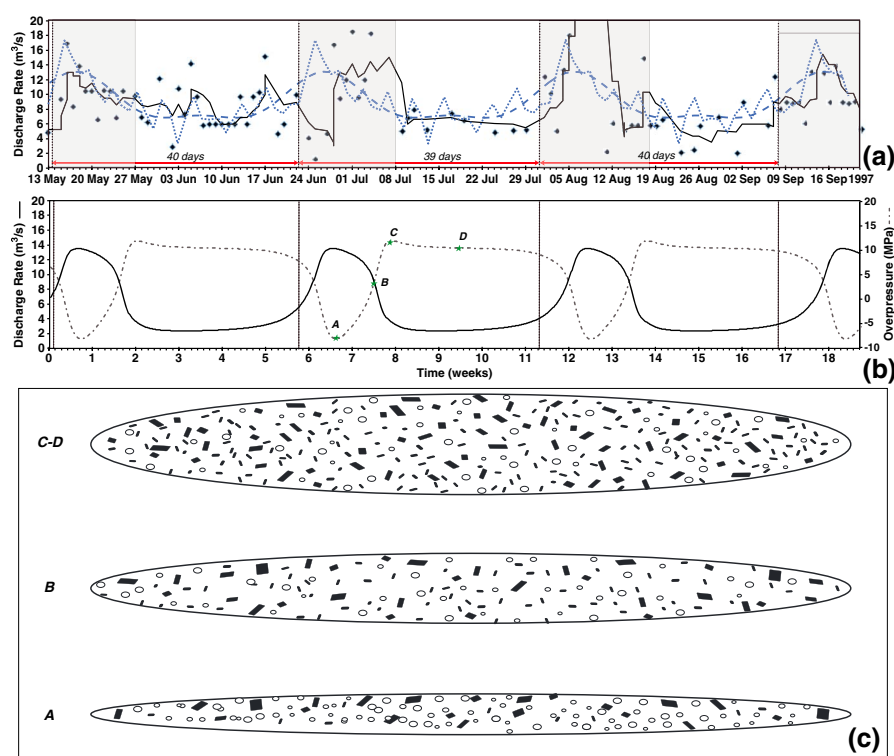
Figure 4. (a) Observed daily lava extrusion rates from 13 May to 21 September 1997 (diamonds) [data modified from *Sparks et al.*, 1998] and the corresponding 4 day moving average curve shown as the black line. The uncertainty on the rates is approximately 30%–50% [*Wadge et al.*, 2010]. The second-order (blue dashed line) and the tenth-order (blue dotted line) expansions of the best fit Fourier series are also shown. The beginnings of four cycles are shown as vertical lines and the period of hybrid swarms by the gray panels. (b) Temporal variation of the model discharge rate at the base of the cylindrical region of the conduit for a ~40 day cycle obtained from the *Costa et al.* [2007a] model using parameters described in Table 1. The corresponding temporal variation of magmatic overpressure in the model is shown as a dash-dot line. (c) The three ellipses represent schematically the horizontal cross sections of crystal and bubble content through the dyke at four states (A, B, C, and D) of the cycle.

high spine appeared on the lava dome; and by 17 May, the direction of growth had switched from S to N [*Watts et al.*, 2002]. The period of intense hybrid swarm activity stopped around 27 May. There was a relative lull in surface extrusive activity from 6 to 13 June [*Loughlin et al.*, 2002]. The production of a spine 3 days after hybrid seismicity started suggests that a more viscous plug of magma had been generated in the conduit during slower magma rise (at the end of the previous cycle) and moved upward for 3 days as a result of higher conduit pressure at its base.

4.2. 22 June–31 July 1997

[15] Marked by an initial swarm of hybrid seismicity on 22 June 1997, subsequent swarms peaked on 24 June [*Loughlin et al.*, 2002]. At approximately 1300 h on 25 June, a collapse of the lava dome following continuous tremor shed a volume of about $5 \times 10^6 \, m^3$ (dense rock equivalent) in three pulses, producing fatal pyroclastic flows. The hybrid seismicity ended by 8 July, coincident with a reduction in tiltmeter-measured deflation [*Sparks and Young*, 2002]. From 8 to 13 July, there was intense ash emission, peaking at the top of each subdaily cycle [*Druitt et al.*, 2002]. From then to the end of July, activity was generally low.

4.3. 31 July–8 September 1997

[16] Low-frequency seismic events restarted on 31 July 1997 [*Voight et al.*, 1999]. Rapid growth of a west-facing lava lobe ended in a $7 \times 10^6 \, m^3$ collapse on 3 August, producing pyroclastic flows that destroyed the town of Plymouth. Starting on 4 August, a series of 13 vulcanian explosions marked the peak of many of the subdaily cycles [*Druitt et al.*, 2002]; but by 13 August, a new lava lobe was established. The intense swarms of hybrid earthquakes ended on 19 August, after which activity was lower. Intense hybrid earthquake swarms resumed on 8 September, by which time extrusion had moved from west to north with more vigorous lava flow.

4.4. Magma Flux–Extrusion Rate

[17] Figure 4a shows the estimated lava extrusion rates for the three consecutive multiweek cycles. These estimates have higher levels of uncertainty at the highest rates, when large pyroclastic flows are being generated [*Wadge et al.*, 2010]. We take the start of the series of intense swarms of hybrid earthquakes as the beginning of each cycle, which defines their periods to be 40, 39, and 40 days. The observed extrusive rates reach peaks ~8 days from the start of the cycle, near the middle of the ~16 day period of hybrid swarms.

[18] Within a few days of the start of the cycle, a change in the direction of lava extrusion (16 May, 8 September) and/or a major collapse of the lava dome (25 June, 3 August) may occur. Both of these are interpreted to be the result of a pulse of magma at high flux reaching the lava dome. In Figure 4b, the simulated magma flux is plotted for a repeating ~40 day cycle (the parameters used are reported in Table 1), together with the magmatic overpressure. The correspondence of the timing of modeled magma flux with the observed lava extrusion is good. The best fit first-order period obtained from a Fourier analysis is 39 days.

[19] The state of the dyke during the cycle is shown schematically in the three ellipses of Figure 4c. In Figure 4cA, after the initial extrusive decompression of the cycle, the dyke is at its narrowest and the magma contains a high proportion of bubbles, enhancing buoyancy. In Figure 4cB, the dyke is expanding as more magma enters than leaves and the bubble fraction has fallen. The dyke reaches its maximum size in Figure 4cC–D, and the bubble fraction is low.

4.5. Periods of Subdaily Cycles

[20] The variations of discharge rate and overpressure shown in Figure 4b affect the variation of other variables that are thought to control subdaily period variability [*Costa et al.*, 2012]. The coupled behavior is nonlinear and is largely determined by the variable response of the rigidity of the combined magma-host rock system. Figures 5a–5c show the behavior of four model variables calculated using the *Costa et al.* [2007a] model: differential pressure and differential magma flux (Figure 5a), the rigidity of the system (Figure 5b), and bubble fraction (Figure 5c) through the 40

day cycle. At the start of the cycle, as magma flux increases and pressure in the dyke falls, gas bubbles nucleate and their volume fraction rises from 0.21 to 0.26 (Figure 5c). This peaks after approximately 6 days into the cycle (Figure 4cA) and then falls to 0.19 before increasing slightly again (Figure 4cC). After 16 days, bubble fraction remains nearly constant until the end of the cycle. The differential magma pressure (dP/dt, Figure 5a) and the differential magma flux within the dyke ($Q_{in} - Q_{out}$, Figure 5a) show similar behavior: falling at the start of the cycle, rising to a peak, and then falling again to near constant values after 16 days. However, the curves do show second-order differences that modulate the behavior of the rigidity parameters and cross twice (Figures 4aA and 4aC). The system rigidity γ (Figure 5b), calculated from the *Costa et al.* [2007a] model as explained in the Appendix, represents the response of the dyke-magma system under strain from magma compression and the elasticity (rigidity) of the dyke wall rocks. This varies over about two orders of magnitude in a complex manner. In particular, there are two strong inflections at A and between B and C (Figure 5b).

[21] Figure 6a shows the periods of the subdaily cycles measured using the tiltmeter record for most of the first two multiweek cycles (13 May–22 June, 22 June–31 July) and the start of the third (for which there are tilt data). Generally, the periods recorded by tiltmeter are very similar to those extracted from seismic data (Figure 6a), but with less scatter. Also shown in Figure 6a are the moving average and the variation in the period of subdaily cycles derived from equation (1). In particular, the green points correspond to $T \approx 0.5A/\gamma$ for the values of γ reported in Figure 5b and
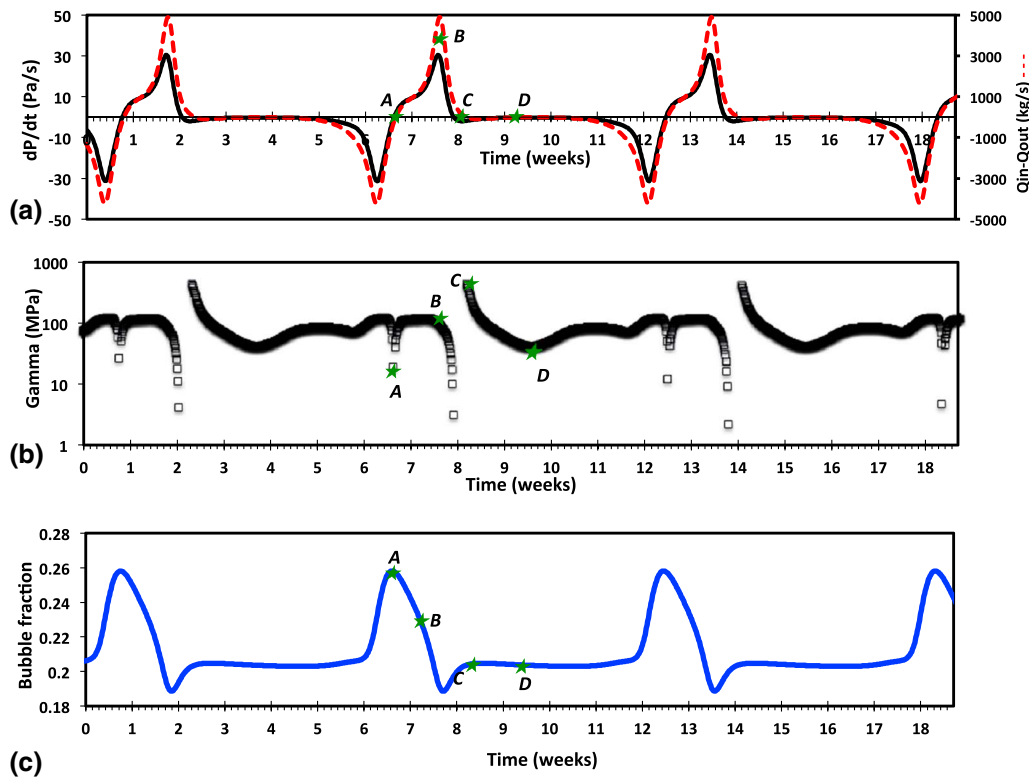

Figure 5. Selected model variable behavior through multiweek (40 day) cycles. (a) Pressure drop and differential magma flux, (b) gamma (rigidity parameter), and (c) bubble fraction.
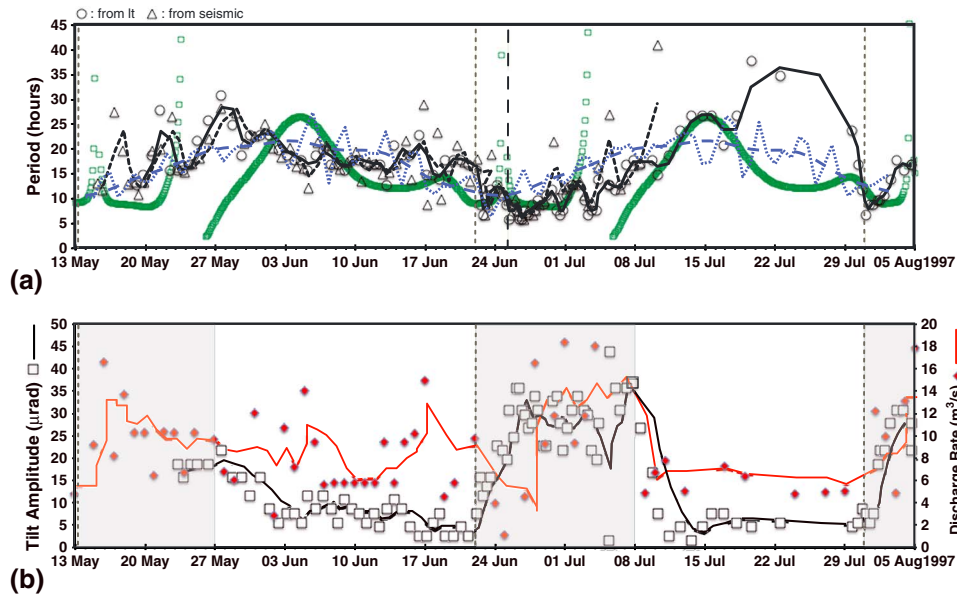
Figure 6. (a) Subdaily periods estimated from both seismic (open triangles) and tilt data (open circles), together with two-day moving average curves (black dashed and bold lines for seismic and tilt data respectively) for two multiweek cycles (starting from vertical dotted lines) from 13 May to 5 August 1997. The second-order (blue dashed line) and the twentieth-order (blue dotted line) expansions of the best fit Fourier series are also shown. The green squares show the periods calculated from equation (1) (see text for details). The vertical solid black lines represent the dome collapses of 25 June and 3 August 1997. (b) Daily variation of tilt amplitude (open black squares) together with a 4-point moving average curve (bold black line). For comparison, the variation of extrusion rate (as in Figure 5) is shown (red full diamonds and curve). The initial periods of observed hybrid swarm activity are shown by the pale gray panels.

the set of parameters in Table 1 (the period in equation (1) was scaled by a factor of 0.5 to better reproduce the averaged value of the observed periods). The complex variation in subdaily period predicted by the model is caused by the nonlinear behavior of the system rigidity parameter as the magmatic gas content changes (Figure 5).

[22] The model yields a reduction in period at the start of the cycle, although smaller than what is often seen (e.g., before 24 June and 31 July 1997). The model then displays two sharp oscillations to higher-period values (e.g., around 14 and 23 May, and 25 June and 3 July 1997, corresponding to Figures 4aA and 4aC). The second of these is not always clear in the data; however, the abrupt variation shown by the model at C may be due to the fact that the *Costa et al.* [2007a] model is not able to properly capture sharp variation around the critical point C because the quasi-static approximation used in equation (1) is not valid there for abrupt variations of γ. In the rest of the modeled cycle, fluctuations in period are more gradual, which is also typically seen in the record. Fourier analysis of the period time-series gives a first-order best fit period of 41 days. It is worth noting that sharp variations at the beginning of the cycle cannot be reproduced even with a high-order Fourier series that do, however, capture long period modulations and higher-frequency variations for the rest of the cycle.

4.6. Amplitudes of Subdaily Cycles

[23] Variation in amplitude of the tilting associated with the subdaily cycles for the 1997 multiweek record is shown in Figure 6b. The beginnings of the 22 June–31 July 1997 and the 31 July–8 September cycles correspond to abrupt

increases in tilt amplitude. The values reach a plateau and then fall sharply in the case of the 22 June–31 July 1997 cycle, corresponding closely to the duration of the hybrid earthquake swarms and the measured lava extrusion rate (Figure 6b). This suggests that the tilt amplitude is effectively correlated with magma flow rate suggesting the control of shear traction on ground deformation near the vent [*Green et al.*, 2006; *Anderson et al.*, 2010], at least during the initial phase of the cycle.

5. Discussion

[24] The coupling of two models that separately simulated subdaily and multiweek cyclicity at SHV produces results that are consistent with the combined understanding of the physical operation of the magma supply system. A vertical, elastic-walled dyke stores compressible magma arriving from below and discharges it into a cylindrical conduit. Flow in the cylinder is pulsatory at a subdaily timescale because of stick-slip behavior near the conduit walls. At the start of the multiweek cycle, the average extrusion rate is high, the period of the subdaily cycle is low, and the amplitude of recoverable, near-field deformation is high. After approximately 16 days of a typical 40 day cycle (0.4 of the cycle), the extrusion rate falls, and the dyke starts to repressurize. This highly asymmetrical behavior of the multiweek cycle is captured well by the models.

[25] Some of the second-order detail of the multiweek models matches the observations less well. For example, the onset of the multiweek cycle can be abrupt—more so than the model onset. One way to achieve a more abrupt

onset is via a failure event. Brittle failure, in the form of slip on fault surfaces along the conduit margin, may play a role. Accounting for a state-dependent friction law in the model development would be required to simulate this. The modeled change in shape of the dyke is elastic and does not involve horizontal lengthening. If the recharge period of the dyke were to lead to a sudden propagation of the dyke horizontally, then the sudden pressure reduction could lead to bubble nucleation and rapid magma ascent, initiating the new cycle. There is no strong, general evidence for volcano-tectonic earthquakes immediately preceding the hybrid earthquake swarms that often denote rapid magma rise at the start of multiweek cycles, but there are some possible instances. For example, on 22 June 1997, at the start of the 22 June–31 July 1997 cycle, there was a set of six volcano-tectonic events immediately preceding the first hybrid swarm.

[26] What causes the variability between multiweek cycles? The extrusion rate data of Figure 4 shows that the 31 July–8 September 1997 cycle was apparently much more peaked than the 13 May–22 June 1997 cycle with its more even rate profile. Both have periods of 40 days and similar volumes (33×10^6 and $30 \times 10^6 \, \mathrm{m}^3$, respectively). This difference may be due to a variable dyke extension, a variable deep magma supply rate into the dyke [*Costa et al.*, 2007b], or perhaps that the extrusion rate data are too uncertain.

[27] Forcing of the system by discrete (external) events will also lead to unmodeled perturbations of repeating mechanisms. Lava dome collapse events of sufficient volume can perturb the pressure throughout the system [*Pinel and Jaupart*, 2005]. There were two such events during the period used here, on 25 June and 3 August 1997. They removed volumes of approximately 5×10^6 and $7 \times 10^6 \, \mathrm{m}^3$, reducing the height of the dome by approximately 100 and 150 m, respectively. *Costa et al.* [2012] showed how such unloading events might cause the system to respond by reducing the subdaily period, as observed. Sensitivity analysis of the model parameters during such forcing may help to refine the physical understanding of the system.

[28] The release of gas from the magma is modeled as a steady process, without any lateral escape or explicit mechanisms such as temporary fracture networks enabling gas transport at much higher than normal rates. The operation of such mechanisms, particularly when coupled with other events such as dome collapse, may lead to other unmodeled perturbations of the cycle.

[29] Divergence between model and observations can be due to the assumptions implicit in equation (1) that is in turn based on the simplified model proposed by *Costa et al.* [2012]. Although the level of model coupling used here reproduces some of the observed features, a better representation of the stick-slip mechanism interacting with the dyke capacitor, generated by future work, may give more realistic results.

6. Conclusions

[30] 1. Coupling two previously tested models of storage and flow of magma at hourly and weekly timescales captures the first-order cyclic behavior at SHV.

[31] 2. The nonlinear variation of the rigidity modulus of the system and the bubble content dominate the dynamics of the subdaily cycles.

[32] 3. The multiweek cycle is asymmetrical, the first 40% of which consists of high rates of lava extrusion during short period/high amplitude subdaily cycles as the dyke reservoir discharges itself. The remainder of the cycle involves increasing pressurization as more magma is stored, accompanied by a gradual increase in the period of the subdaily cycles. The model captures well the main features.

[33] 4. The combined model does not capture well the abrupt start of the multiweek cycles. This may indicate other mechanisms and require more sophisticated models.

Appendix A: Numerical Calculation of the System Rigidity

[34] In this appendix, we describe how we estimated the values of the system rigidity parameter, γ, reported in Figure 5b.

[35] We estimated γ using the *Costa et al.* [2007a] model and the parameters reported in Table 1. From equation (1) in *Costa et al.* [2012], γ can be written as

$$\gamma \approx \frac{<\rho><V_\mathrm{d}>}{(Q_\mathrm{in}-Q_\mathrm{out})}\frac{\mathrm{d}P_*}{\mathrm{d}t} \approx \frac{<\rho><V_\mathrm{d}>\,\mathrm{sgn}(Q_\mathrm{in}-Q_\mathrm{out})}{\sqrt{(Q_\mathrm{in}-Q_\mathrm{out})^2+\varepsilon^2}}\frac{\mathrm{d}P_*}{\mathrm{d}t}$$

where $<\rho>$ is the averaged magma density obtained by integration of the local density along the dyke, $<V_\mathrm{d}>$ is the average volume of the dyke, P_* is the overpressure at the top of the dyke, Q_in is the mass influx into the dyke, Q_out the mass influx into the cylinder, and ε is a small numerical regularization constant (with $\varepsilon/(Q_{in} \approx 10^{(-3)})$).

References

Anderson, K., M. Lisowski, and P. Segall (2010), Cyclic ground tilt associated with the 2004-2008 eruption of Mount St. Helens, *J. Geophys. Res.*, *112*, doi:10.1029/2009JB007102.

Costa, A., O. Melnik, R. Sparks, and B. Voight (2007a), Control of magma flow in dykes on cyclic lava dome extrusion, *Geophys. Res. Lett.*, L02303, doi:10.1029/2006GL027466.

Costa, A., O. Melnik, and R. S. J. Sparks (2007b), Controls of conduit geometry and wallrock elasticity on lava dome eruptions, *Earth Planet. Sci. Lett*, *260*, 137–151, doi:10.1016/j.epsl.2007.05.024.

Costa, A., G. Wadge, and O. Melnik (2012), Cyclic extrusion of a lava dome based on a stick-slip mechanism, *Earth Planet. Sci. Lett.*, *337–338*, 39–46, doi:10.1016/j.epsl.2012.05.011.

Denlinger, R. P., and R. P. Hoblitt (1999), Cyclic eruptive behaviour of silicic volcanoes, *Geology*, *27*, 459–462.

Druitt, T. H., et al. (2002), Episodes of cyclic vulcanian explosive activity with fountain collapse at Soufriere Hills Volcano, Montserrat, in The eruption of Soufriere Hills Volcano, Montserrat, Montserrat, from 1995–1999, vol **21**, edited by T.H Druitt, and B.P Kokelaar, pp. 281–306, Geological Society, London, Memoirs.

Elsworth, D., G. Mattioli, J. Taron, B. Voight, and R. Herd (2008), Implications of magma transfer between multiple reservoirs on eruption cycling, *Science*, *322*, 246–248, doi:10.1126/science.1161297.

Green, D. N., and J. Neuberg (2006), Waveform classification of volcanic low-frequency earthquake swarms and its implication at Soufriere Hills Volcano, Montserrat, *J. Volcanol. Geotherm. Res.*, *153*, 51–63.

Green, D. N., J. Neuberg, and V. Cayol (2006), Shear stress along the conduit wall as a plausible source of tilt at Soufriere Hills volcano, Montserrat, *Geophys. Res. Lett.*, *33*, L10306, doi:10.1029/2006GL025890.

Hautmann, S., J. Gottsmann, R. S. J. Sparks, A. Costa, O. Melnik, and B. Voight (2009), Modelling ground deformation response to oscillating overpressure in a dyke conduit at Soufriere Hills volcano, Montserrat, *Tectonophysics*, *471*, 87–95.

Lensky, N. G., R. S. J. Sparks, O. Navon, and V. Lyakhovsky (2008), Cyclic activity at Soufriere Hills Volcano, Montserrat: Degassing-induced pressurization and stick-slip extrusion. in Fluid Motions in Volcanic Conduits: A Source of Seismic and Acoustic Signals, vol. 307, edited by S. J Lane, and J. S Gilbert, pp. 169–188, Geological Society Special Publication, London, U. K.

Loughlin, S. C., et al. (2002), Pyroclastic flows and surges generated by the 25 June 1997 dome collapse, Soufriere Hills Volcano, Montserrat. in The eruption of Soufriere Hills Volcano, Montserrat, from 1995–1999, edited by T.H. Druitt, and B.P Kokelaar, vol 21, pp. 191–209, Geological Society, London, Memoirs.

Luckett, R., S. Loughlin, S. De Angelis, and G. Ryan (2008), Volcanic seismicity at Montserrat, a comparison between the 2005 dome growth episode and earlier dome growth, *J. Volcanol. Geotherm. Res.*, 177, 894–902.

Melnik, O., and R. S. J. Sparks (1999), Nonlinear dynamics of lava dome extrusion, *Nature*, 402, 37–41.

Melnik, O, R. S. J. Sparks, A. Costa, and A. Barmin (2009), Volcanic Eruptions: Cyclicity During Lava Dome Growth. in Encyclopedia of Complexity and Systems Science, Editor in chief: R.A. Meyers, 10995 pp, vol. 11, pp. 9763–9784, Springer, Berlin, doi:10.1007/978-0-387-30440-3_578.

Neuberg, J. W., H Tuffen, L. Collier, T. Powell, and D. Dingwell (2006), The trigger mechanism of low-frequency earthquakes on Montserrat, *J. Volcanol. Geotherm. Res.*, 153, 37–50.

Nishi, K, M. Hendrasto, I. Mulyana, U. Rosadi, and M. A. Purbawinata (2007), Micro-tilt changes preceding summit explosions at Semeru volcano, Indonesia, *Earth Planets Space*, 59, 151–156.

Odbert, H. M., and G. Wadge (2009), Time series analysis of lava flux, *J. Volcanol. Geotherm. Res.*, 188(4), 305–314.

Odbert, H. M., R. C. Stewart, and G. Wadge (2013), Cyclic phenomena at the Soufriere Hills Volcano, Montserrat. in The eruption of Soufriere Hills Volcano, Montserrat from 2000–2010, edited by G Wadge, B Voight, and R Robertson, Geological Society, London, Memoirs (accepted).

Paulatto, M., et al. (2009), Upper crustal structure of an active volcano from refraction/reflection tomography, Montserrat, Lesser Antilles, *Geophys. J. Int.*, 180, 685–696, doi:10.1111/j.1365-246X.2009.04445.x.

Paulatto, M., C. Annen, T. J. Henstock, E. Kiddle, T. A. Minshull, R. S. J. Sparks, and B. Sparks (2012), Magma chamber properties from integrated seismic tomography and thermal modelling at Montserrat, *Geophys. Geochem. Geosys.*, 13, Q011014.

Pinel, V, and C. Jaupart (2005), Some consequences of volcanic edifice destruction for eruption conditions, *J. Volcanol. Geotherm. Res.*, 145, 68–80.

Sparks, R. S. J., et al. (1998), Magma production and growth of the lava dome of the Soufriere Hills Volcano, Montserrat, West Indies: November 1995 to December 1997, *Geophys. Res. Lett.*, 25, 3421–3424.

Sparks, R. S. J., and S. R. Young (2002), The eruption of Soufriere Hills Volcano, Montserrat (1995-1999): overview of scientific results. in The eruption of Soufriere Hills Volcano, Montserrat, from 1995–1999, edited by T.H Druitt, and B.P Kokelaar, vol 21, pp, 45–69, Geological Society, London, Memoirs.

Thomas, M. E., and J. Neuberg (2012), What makes a volcano tick–a first explanation of deep multiple seismic sources in ascending magma, *Geology*, 40, 351–354.

Voight, B., R. P. Hoblitt, A. B. Clarke, A. B. Lockhart, A. D. Miller, L. Lynch, and J. McMahon (1998), Remarkable cyclic ground deformation monitored in real-time on Montserrat, and its use in eruption forecasting, *Geophys. Res. Lett.*, 25, 3405–3408.

Voight, B., et al. (1999), Magma flow instability and cyclic activity at Soufrière Hills Volcano, Montserrat, *Science*, 283, 1138–1142.

Watts, R. B., R. A. Herd, R. S. J. Sparks, and S. R. Young (2002), Growth patterns and emplacement of the andesitic lava dome at Soufriere Hills Volcano, Montserrat. in The eruption of Soufriere Hills Volcano, Montserrat, from 1995–1999, edited by T.H Druitt, and B.P Kokelaar, vol 21, pp. 115–152, Geological Society, London, Memoirs.

Wadge, G., R. Herd, G. Ryan, E. S. Calder, and J.-C. Komorowski (2010), Lava production at Soufriere Hills Volcano, Montserrat: 1995-2009, *Geophys. Res. Lett.*, 37, L00E03.

Wylie, J. J., B Voight, and J. A. Whitehead (1999), Instability of magma flow from volatile-dependent viscosity, *Science*, 285, 1883–1885.

Wang, Z. (2000), Dynamic versus static elastic properties of reservoir rocks, SEG Books, 19, 531–539.

Yamashina, K., T. Matsushima, and S. Ohmi (1999), Volcanic deformation at Unzen, Japan, visualized by a time-differential stereoscopy. *J. Volcanol. Geotherm. Res.*, 89, 73–80.